Highly-efficient hydroxyapatite-supported nickel catalysts for dry reforming of methane

Bruna Rêgo de Vasconcelos, Doan Pham Minh, Emmanuel Martins, Alain Germeau, Patrick Sharrock, Ange Nzihou

Highly-efficient hydroxyapatite-supported nickel catalysts for dry reforming of methane

Bruna Rego de Vasconcelos [a,c], *Doan Pham Minh* [a,b,*], *Emmanuel Martins* [d], *Alain Germeau* [d], *Patrick Sharrock* [a], *Ange Nzihou* [a]

[a] *Université de Toulouse, IMT Mines Albi, UMR CNRS 5302, Centre RAPSODEE, Campus Jarlard, F-81013, Albi Cedex 09, France*

[b] *Institute of Research and Development, Duy Tan University, Da Nang 550000, Viet Nam*

[c] *Biomass Technology Laboratory, Department of Chemical and Biotechnological Engineering, Université de Sherbrooke, Sherbrooke, Québec, Canada, J1K 2R1*

[d] *PRAYON S.A., Rue J. Wauters, 144, B-4480, Engis, Belgium*

HIGHLIGHTS

- Hydroxyapatite-based (HAP) catalyst was investigated in dry reforming of methane.
- High temperature (above 700 °C) was crucial for CO_2 and CH_4 conversions.
- Atmospheric pressure also favored dry reforming of methane reaction.
- Hydroxyapatite-based catalyst was active, selective and stable at 700 °C for 90 h.
- Sintered HAP could be used as catalyst support without further thermal sintering risk.

Keywords:
Dry reforming of methane
Hydrogen
Syngas
Hydroxyapatite
Nickel catalyst

ABSTRACT

Ni-based catalysts were prepared using two hydroxyapatites (Ca-HA1, S_{BET} = 7 m^2/g and Ca-HA2, S_{BET} = 60 m^2/g) with different physico-chemical properties. The objective of the study was to evaluate the performance of these two materials as promising supports for dry reforming reaction (DRM) as well as to investigate the influence of different process parameters, such as temperature, pressure, time and catalyst pretreatment on the performance of these two catalysts. Thermodynamic calculations were performed to determine the conditions that would limit solid carbon deposit and favor the reactants conversion. Then, an experimental parametric study was carried out to investigate the impact of the temperature, pressure, catalyst pretreatment and support thermal treatment on the catalysts performance. The results showed that the catalyst pretreatment allowed the reduction of the nickel particles in a higher extent, which resulted in better catalytic performance when compared to the catalysts without pretreatment. High temperatures around 700 °C and low pressures around 1.6 bar were required to attain high CH_4 and CO_2 conversions around 70–80% as well as high H_2 and CO selectivity around 90% for 90 h of time on stream. In all cases, Ni/Ca-HA2 catalyst presented better catalytic performance than Ni/Ca-HA1 due to the presence of smaller nickel particles (10–20 nm), stronger basicity, higher density of basic sites (0.23 mmol g^{-1}) as well as higher specific surface area (S_{BET} = 60 m^2/g) of the Ca-HA2 support. Ni/Ca-HA2 catalyst was highly active (initial methane conversion: 75%) and relatively stable during 90 h of TOS and its catalytic

* *Corresponding author*. Université de Toulouse, IMT Mines Albi, UMR CNRS 5302, Centre RAPSODEE, Campus Jarlard, F-81013, Albi cedex 09, France.
E-mail address: doan.phamminh@mines-albi.fr (D. Pham Minh).

Introduction

The increase in the greenhouse gases (GHG) emissions along with the depletion of carbon-based energy resources have forced scientists to develop new technologies and processes for the substitution of fossil fuels by other types of energies. Synthetic gas (syngas), which is a mixture of CO and H_2, is an important platform chemical that has an energy density of about 50% of natural gas [1] and has been used for illumination of cities as well as for heat and power generation at industrial scale [2]. More importantly, syngas can be used as feedstock for the production of value-added chemicals, such as methanol, ammonia, dimethyl ether and even liquid fuels through Fischer-Tropsch synthesis (FTS) [3].

Syngas can be obtained by steam reforming and partial oxidation of hydrocarbons, such as methane, propane, etc [4]. However, steam reforming is an energy intensive process and faces corrosion problems. Partial oxidation also faces several issues, such as hot spots in the catalyst bed, which can lead to catalyst deactivation [5]. Dry reforming of hydrocarbon is a similar process also allowing the production of syngas that has gained increased interest in the last decade due to its environmental advantages. The stoichiometric reaction of dry reforming of methane (DRM) is given in the Eq. (1). This reaction converts CO_2 and CH_4, which are the two main greenhouse gases, into syngas with H_2/CO ratio close to 1, which is suitable for FTS of hydrocarbons [6] as well as for synthesis of important energy vectors, such as methanol [7]. It is also an environmentally friendly way for biogas, landfill and natural gas valorization, in which the content of CH_4 is around 50–65% (for biogas and landfill gas) and 90% (for natural gas) [5,8]. In fact, it is possible to prepare a mixture containing 50 mol% of CH_4 and 50 mol% of CO_2 according to Eq. (1), by using CO_2 from carbon dioxide capture processes, to feed DRM process.

$$CH_4 + CO_2 \leftrightarrow 2H_2 + 2CO \quad \Delta H_{298} = 247\ kJ{\cdot}mol^{-1} \tag{1}$$

Despite the environmental benefits of this reaction, DRM has not reached the industrial scale yet mainly due to the rapid deactivation of the catalysts by sintering and coke deposition. In fact, because of its high positive reaction enthalpy, high temperature above 700 °C is required to achieve high reactants' conversion. The high temperature required for the reaction may lead to catalyst sintering (support and active phase and, consequently, catalyst deactivation. In addition, several side reactions that generate solid carbon and water as undesirable byproducts also occur, leading to catalyst deactivation. These reactions are listed below (Eqs. (2)–(5)):

$$\text{Reverse water} - \text{gas shift: } \mathbf{CO_2 + H_2 \leftrightarrow H_2O + CO} \quad \Delta H_{298} = 41\ \mathbf{kJ{\cdot}mol^{-1}} \tag{2}$$

$$\text{Boudouard reaction: } \mathbf{2CO \leftrightarrow C + CO_2} \quad \Delta H_{298} = -172\ \mathbf{kJ{\cdot}mol^{-1}} \tag{3}$$

$$\text{Methane cracking: } \mathbf{CH_4 \leftrightarrow C + 2H_2} \quad \Delta H_{298} = 75\ \mathbf{kJ{\cdot}mol^{-1}} \tag{4}$$

$$\text{Steam gasification of carbon: } \mathbf{C_{(s)} + H_2O \leftrightarrow CO + H_2} \quad \Delta H_{298} = 131\ \mathbf{kJ{\cdot}mol^{-1}} \tag{5}$$

Several papers and reviews have been published with different approaches to minimize coke deposition [5,9–12]. The most frequently reported are: optimization of reaction conditions (temperature, pressure, flow rate etc.) and development of coke-resistant catalysts. The first approach requires high temperatures, low pressures and low space velocities in order to keep the reaction at high reactants conversion as well as high selectivity to syngas (CO and H_2) for long periods of time. The second approach can be achieved by using suitable supports with high surface area to allow high dispersion of the active phase as well as the formation of small metallic particles (<15 nm) that can limit the growth of filamentous carbon, which will later lead to catalytic deactivation [5,13]. Highly-dispersed metal particles, such as Ni, Co, Fe, Pt and Ru particles have been extensively reported as promising active phases for DRM catalysts [3]. The metal-support interaction is also an important parameter. The metal-support interaction should be strong enough to prevent sintering of the active phase during the reaction, which will also lead to catalytic deactivation, but not too strong, which would hinder the reduction active phase [3,5,11,14,15]. The presence of basic sites is also an important since it will improve the CO_2 adsorption and favor the coke removal via Eq. (5) [5,16–18].

Calcium-hydroxyapatite ($Ca_{10}(PO_4)_6(OH)_2$), named thereafter Ca-HA, is a good candidate for the synthesis of catalysts for DRM process. In fact, hydroxyapatite has the ability to undergo cation and anion exchanges, which can improve its surface properties [19–21]. Also, its acid-base properties could be controlled by modifying the calcium to phosphorous ratio (Ca/P) [22]. Ca-HA is also thermally stable, decomposing only at temperatures above 1000 °C and no sintering is observed under 700 °C [23]. Due to these properties, Ca-HA has been used as catalyst support in various chemical reactions, such as water-gas-shift reaction [24], methane oxidation [25], steam reforming of glycerol [26] etc and promising results have been obtained when compared to catalysts prepared with conventional supports. To the best of our knowledge, only Boukha et al. [27] and our team [4] have investigated Ca-HA based catalysts for DRM process. However, the physico-chemical properties of the hydroxyapatite used by Boukha et al. [27] were quite different from the ones presented in this

manuscript, especially regarding the specific surface area, Ca/P ratio, basicity etc.

In this work, catalysts containing nickel as active phase and Ca-HA as support were synthesized and evaluated in DRM. Two Ca-HA with different physico-chemical properties developed by our industrial partner were used. The influence the temperature, pressure and catalyst pretreatment was investigated. Particularly, for the first time, in order to avoid any sintering of the supports, a thermal treatment of the supports at high temperature was performed and the performance of the catalysts prepared on these thermally treated supports was compared with those without thermal treatment. Surprisingly, the catalysts prepared on thermally treated supports showed high catalytic activity, selectivity and stability despite their low specific surface area (<2 m^2/g). This is also a novelty of this work which can be a key for the development of a stable catalyst for DRM process.

Experimental

Catalyst preparation

Two hydroxyapatites, Ca-HA1 (S_{BET} = 7 m^2g^{-1}, d_{50} = 5.2 μm) and Ca-HA2 (S_{BET} = 60 m^2g^{-1}, d_{50} = 6.1 μm), developed and provided by PRAYON (Belgium), were used as catalytic supports. The objective of using two hydroxyapatites with different specific surface areas (S_{BET}) was to investigate the influence of the S_{BET} on the nickel particles distribution, and, consequently, on the catalyst performance. Both supports were used as received and then doped with nickel by incipient wetness impregnation technique using an aqueous solution of $Ni(NO_3)_2$ (>98%, Fisher Scientific) [5]. Residual water was removed by drying at 105 °C overnight. No calcination step was performed since the water and nitrates present in the catalyst decompose at temperatures lower than 400 °C, which is the initial reaction temperature (Fig. S1). The theoretical nickel content was 5.7 wt% for each catalyst. The catalysts are called thereafter Ni/Ca-HA1 and Ni/Ca-HA2.

The influence of the support thermal treatment was also investigated. In this case, both supports were first heated at 1000 °C under air atmosphere for 5 h. Then, the supports doped with nickel using the same method as for the catalysts without thermal treatment. The catalysts are called thereafter Ni/Ca-HA1_S and Ni/Ca-HA2_S.

Catalytic reaction

DRM process was performed with a fixed-bed reactor of internal diameter of 8 mm. For each test, the dried powder catalyst (300 mg) was diluted twice with inert and non-porous alumina powder (purchased from TOPSOE). The reactor was then filled with the first layers of alumina powder, followed by the mixture of catalyst/alumina powder prepared above which was positioned at the center of the reactor, and finally with the second layer of alumina powder. Micrometric particles of catalyst and alumina created a pressure drop of 0.6 bar inside the reactor. A thermocouple allows measuring and controlling the reaction temperature at the center of the catalyst bed. For DRM reaction, the reactor was fed with a synthetic gas mixture of the following composition: 20 mol% of CH_4, 20 mol% of CO_2 and 60 mol% of N_2 with a weight hour space velocity (WHSV) of 15.9 L h^{-1} g_{cat}^{-1}. Water in the outlet gas mixture was periodically quantified by silica gel in a glass-tube. Taking into account the stoichiometry of Eqs. (1)–(5), the total gas flow rate at the reactor outlet evolves compared to inlet flow rate. Thus, it was determined by a gas counter. This measurement was crucial to calculate the conversion and selectivity of the reaction, according to Eqs. (6)–(10) below. The composition of outlet gas mixture was performed with a μ-GC (A3000, Agilent).

$$CH_4\ \text{conversion}(\%) = \frac{\dot{Q}_{(CH_4)_{in}} - \dot{Q}_{(CH_4)_{out}}}{\dot{Q}_{(CH_4)_{in}}} x100 \quad (6)$$

$$CO_2\ \text{conversion}(\%) = \frac{\dot{Q}_{(CO_2)_{in}} - \dot{Q}_{(CO_2)_{out}}}{\dot{Q}_{(CO_2)_{in}}} x100 \quad (7)$$

$$H_2O\ \text{selectivity}(\%) = \frac{\dot{Q}_{O_{(H_2O\ \text{produced})}}}{\dot{Q}_{O_{(CO_2\ \text{consumed})}}} x100 \quad (8)$$

$$CO\ \text{selectivity}\ (\%) = \frac{\dot{Q}_{O_{(CO\ \text{produced})}}}{\dot{Q}_{O_{(CO_2\ \text{consumed})}}} x100 \quad (9)$$

$$H_2\ \text{selectivity}\ (\%) = \frac{\dot{Q}_{H_{(H_2\ \text{produced})}}}{\dot{Q}_{H_{(CH_4\ \text{consumed})}}} x100 \quad (10)$$

$$C_{(s)}\ \text{selectivity}(\%) = \frac{\dot{Q}_{CS_{(out)}}}{\dot{Q}_{C_{(CH_4\ \text{consumed})}} + \dot{Q}_{C_{(CO_2\ \text{consumed})}}} x100 \quad (11)$$

where $\dot{Q}$ means gas flow rate; *in* means inlet; *out* means outlet.

For the parametric study, the temperature and total pressure of the reaction were varied from 400 to 700 °C and from 1 to 25 bar, respectively. The effect of catalyst pretreatment was also investigated by performing an *in-situ* reduction step at 700 °C under 4%H_2/N_2 flow prior to the reaction. The influence of support thermal treatment was studied by heating both supports at 1000 °C for 5 h prior to the impregnation step. Each test was repeated at least twice and the deviation of the analysis was generally smaller than 3%.

Catalyst characterization

N_2 adsorption-desorption isotherms

N_2 adsorption-desorption isotherms were recorded in this work mainly to measure the specific surface area of the supports (Ca-HA1 and Ca-HA2) as well as to evaluate the porosity of the samples, which will later allow to understand their influence on the nickel particles dispersion and on the catalyst performance. The supports were initially degassed for 24 h at 105 °C below 100 mbar. BET measurements were then performed using Tristar II 3020 from Micromeritics at 77 K.

CO_2-Temperature-programmed desorption (CO_2-TPD)

CO_2-Temperature-programmed desorption (CO_2-TPD) was performed in this work to evaluate the density of basic sites in each support. This is an important analysis since the basicity of a support/catalyst will dictate the CO_2 adsorption on the

catalyst surface. 100 mg of the sample was heated up to 800 °C at the heating rate of 10 °C min^{-1} under He flow and then cooled down to 50 °C. CO_2 chemisorption was then performed at 50 °C under 0.5%CO_2/N_2 flow. After purging the sample under He flow at this same temperature, CO_2-TPD profile was recorded from 50 to 800 °C at the heating rate of 10 °C min^{-1}, using the AutoChem 2920 from Micromeritics.

Temperature-programmed reduction (TPR)
Temperature-programmed reduction (TPR) was used in this work to evaluate not only the temperature of reduction of each catalyst but also their metal-support interaction, which are two important parameters related to the catalyst performance. The analyses were performed in an AutoChem 2920 from Micromeritics. 100 mg of the catalyst sample was initially purged under He flow for 30 min at 100 °C in order to clean the surface of the catalyst. TPR profile of the dried catalyst was recorded from 25 to 850 °C at the heating rate of 10 °C min^{-1} under 5%H_2/N_2 flow.

Inductively coupled plasma - optical emission spectroscopy (ICP-OES)
Inductively coupled plasma - optical emission spectroscopy (ICP-OES) was used in this work to verify the Ca/P ratio of the hydroxyapatite supports as well as to quantify the nickel content of the dried catalysts. First, 100 mg of the dried catalyst was dissolved in an acidic mixture of HNO_3 (33 vol %) and HCl (67 vol%) at 90 °C for 1 h and then diluted 10 times in water. (Jobin Yvon Ultima 2, HORIBA). The measurements were then performed using a Jobin Yvon Ultima 2, HORIBA.

X-ray diffraction (XRD)
X-ray diffraction (XRD) was performed in this work in order to determine the crystalline structure of the catalysts. First, the catalysts were calcined at 500 °C under air for 1 h in order to better identify the crystalline phases that could be formed during the reaction. The analyses were recorded with a X'Pert MPD diffractometer operating with Cu Kα radiation over a 2θ range between 10 and 75°. A scan step size of 0.042°s^{-1} was used.

Thermogravimetric analysis (TG)
Thermogravimetric analysis (TG) was performed to evaluate the thermal behavior of dried catalyst. The analysis (see Supplementary material) were performed at a 100 mL/min air flow at a temperature range of 30–1000 °C and at the heating rate of 5 °C min^{-1}. The equipment SDTQ600 from TA Instruments was used for the analysis.

Environmental Scanning Electron Microscopy (ESEM)
Environmental Scanning Electron Microscopy (ESEM) was used in this work to characterize the shape and size of the nickel particles (or agglomerates) present in each catalyst. The catalysts were first calcined at 500 °C under air for 1 h. The powder was then dispersed on a carbon-based support for direct observation of sample (no coating pretreatment was employed). The analysis were then performed using a XL30 ESEM FEG (Philips) apparatus.

Transmission electron microscopy (TEM)
Transmission electron microscopy (TEM) was used in this work to analyze the size and the distribution of nickel nanoparticles more precisely on the surface of catalyst. The catalysts were previously calcined at 500 °C under air for 1 h. Then, the samples were dispersed into ethanol and submitted to ultrasound for 5 min. After this treatment, the solution was dispersed on a grill, dried and analyzed using ARM200F (Jeol) and XL30 ESEM FEG (Philips) apparatus.

Results

Characterization

Textural properties of supports and fresh catalysts
Fig. 1a,b show the isotherms of nitrogen adsorption-desorption obtained with the initial Ca-HA1 and Ca-HA2 supports, respectively. The shape of both isotherms indicates that they can be assigned to the type II according to the IUPAC classification, which is related to non-porous or macroporous materials [28,29]. Moreover, according to Lowel et al. [30], the limited uptake at low relative pressure indicates the absence of micropores (pore diameter < 2 nm). Ca-HA1 (Fig. 1a) did not show hysteresis loop, so it is a nonporous material. On the other hand, a hysteresis loop was observed at the relative pressure higher than 0.6 for Ca-HA2 (Fig. 1b) signifying the presence of mesopores (pore diameter within 2 and 50 nm) in this material. Accordingly, the specific surface area determined by BET method was 60 m^2 g^{-1} for Ca-HA2 explained by its mesoposity, and was 7 m^2 g^{-1} for nonporous Ca-HA1 (Table 1). The deposition of nickel particles (5.7 wt%) on the surface of these supports had not significant impact on the specific surface area of the initial supports.

CO_2- TPD
The basic properties of the supports was evaluated by CO_2-TPD. The amount of basic sites is represented by the surface under the desorption peaks. On the other hand, the strength of the basic sites is related to the desorption temperature: weak basicity for desorption temperature lower than 200 °C, medium basicity for desorption temperature between 200 and 300 °C, and strong basicity for desorption temperature higher than 300 °C [31–34]. Fig. 2 shows CO_2-TPD profiles of both Ca-HA1 and Ca-HA2 supports.

Ca-HA1 support showed a large desorption peak with the maximum at 140 °C, which indicates the predominance of weak and medium basic sites. However, the CO_2-TPD profile of the Ca-HA2 support was quite different from the one obtained with Ca-HA1. In the case of Ca-HA2 support, two desorption peaks with maximums at 150 and 400 °C were observed. The large surface under the second peak indicates the predominance of strong basic sites in this support, contrarily to the Ca-HA1 support, which presented mainly weak basic sites. The density of basic sites for both supports is summarized in Table 1. As expected, Ca-HA2 presented a higher density of basic sites (0.23 mmol g^{-1}) than Ca-HA1 (0.07 mmol g^{-1}). The results obtained with Ca-HA2 are in accordance with those obtained by Stosic et al. [35] for a stoichiometric hydroxyapatite (Ca/P = 1.67).

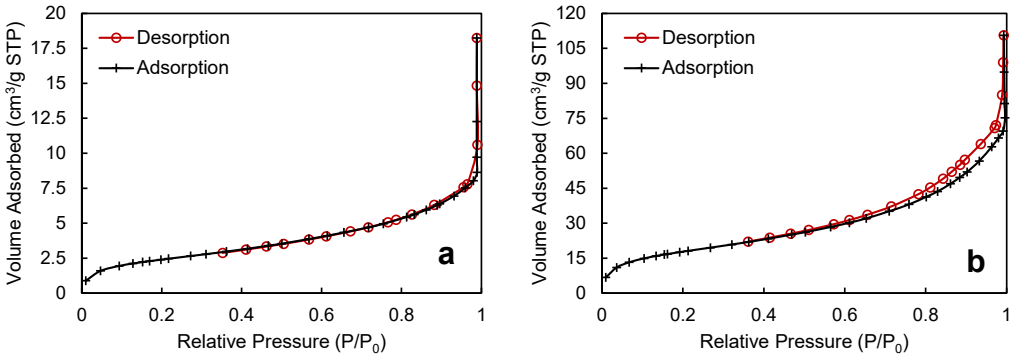

Fig. 1 – Nitrogen adsorption-desorption isotherms of (a) Ca-HA1 and (b) Ca-HA2.

Table 1 – Some properties of the fresh catalysts.

Sample	Textural characterization		ICP-OES			Basicity
	S_{BET} (m^2/g)	V_p (cm^3/g)	Ca/P	Ni content (wt.%), theoretical value	Ni content (wt.%)	Total basicity (mmol/g)
Ca-HA1	7	nd	1.66	–	–	0.07
Ca-HA2	60	0.072	1.67	–	–	0.23
Ni/Ca-HA1	6	–	–	5.7	5	–
Ni/Ca-HA2	57	–	–	5.7	5	–

ICP-AOS analysis

ICP-AOS results are shown in Table 1. The molar ratio of Ca to P was 1.66 and 1.67 for Ca-HA1 and Ca-HA2, respectively. So, Ca-HA1 is slightly deficient in Ca while Ca-HA2 is a stoichiometric hydroxyapatite. About the nickel content of the catalysts, both the catalyst contained 5 wt% of Ni which corresponds to a 88% of nickel deposition yield by the incipient wetness impregnation. This difference is usually observed for the incipient wetness impregnation and must be due to the loss of nickel nitrate during the impregnation step.

XRD analysis

Fig. 3 shows the XRD patterns of the initial supports and calcined catalysts. Both supports showed only the presence of the crystalline phase of hydroxyapatite structure. The main peaks of this crystalline phase were found at 2θ of 31.9, 32.3, 33.0 and 34.1°. For the calcined catalysts, nickel deposition did not notably affect the structure of the initial supports. Diffraction peaks at 2θ of 37, 43 and 63° could be assigned to NiO crystalline phase. Also, no peak of CaO was detected indicating that the exchange between Ni^{2+} and Ca^{2+} of the apatitic structure did not significantly occurred and could not be detected by XRD.

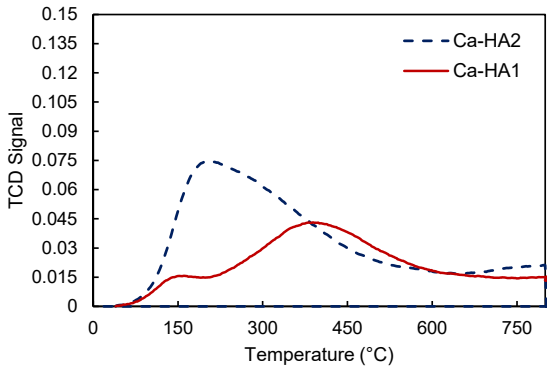

Fig. 2 – CO_2-TPD profiles of the supports used in this work.

Transmission electron microscopy (TEM)

Fig. 4 illustrates TEM images of the calcined catalysts (Ni/Ca-HA1 and Ni/Ca-HA2). The morphology of the catalysts was very different to each other. Ni/Ca-HA1 catalyst (Fig. 4a,b) presented large nickel particles (≈100–200 nm), which could be partially attributed to the low specific surface area of Ca-HA1 support [5] (Table 1). As expected, the Ni/Ca-HA2 catalyst presented much smaller nickel particles in the range of 10–20 nm (Fig. 4c,d), which can be mainly attributed to its higher specific surface area, as presented in Table 1. Numerous studies have reported the high specific surface area of the supports as the key factor for obtaining highly dispersed and small nickel particles [5,10,11,36,37]. This is indeed an important parameter to take into consideration during the preparation of catalysts since it is, along with metal-support interaction one of the factors allowing high activity, stability and resistance against carbon formation and sintering [5,10,11,36,37]. Mesopores could also be observed on the surface of the Ca-HA2 support, which was consistent with the nitrogen adsorption-desorption isotherms results previously presented (Fig. 1).

Temperature programmed reduction (H_2-TPR)

TPR profiles of the calcined catalysts are presented in Fig. 5. For Ni/Ca-HA1, three distinct broad peaks were observed with maximum at 368, 397 and 409 °C. For Ni/Ca-HA2, two sharp

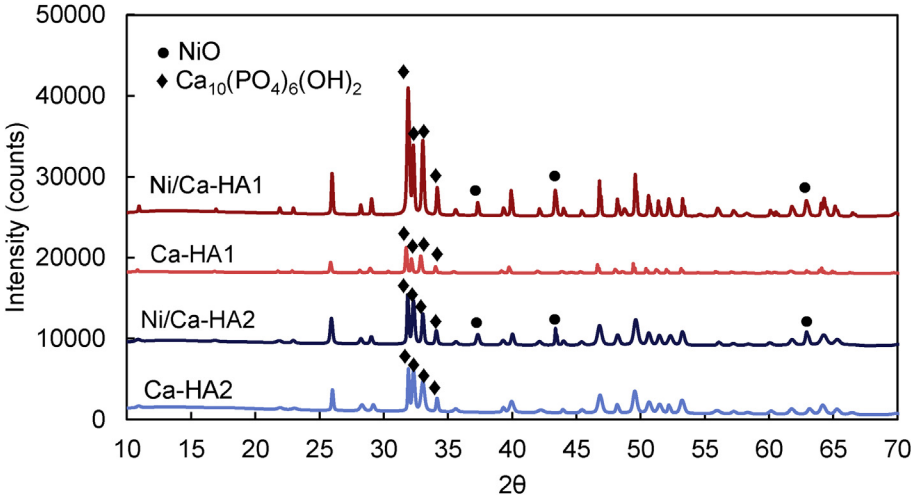

Fig. 3 – XRD patterns of supports and nickel catalysts calcined at 500 °C.

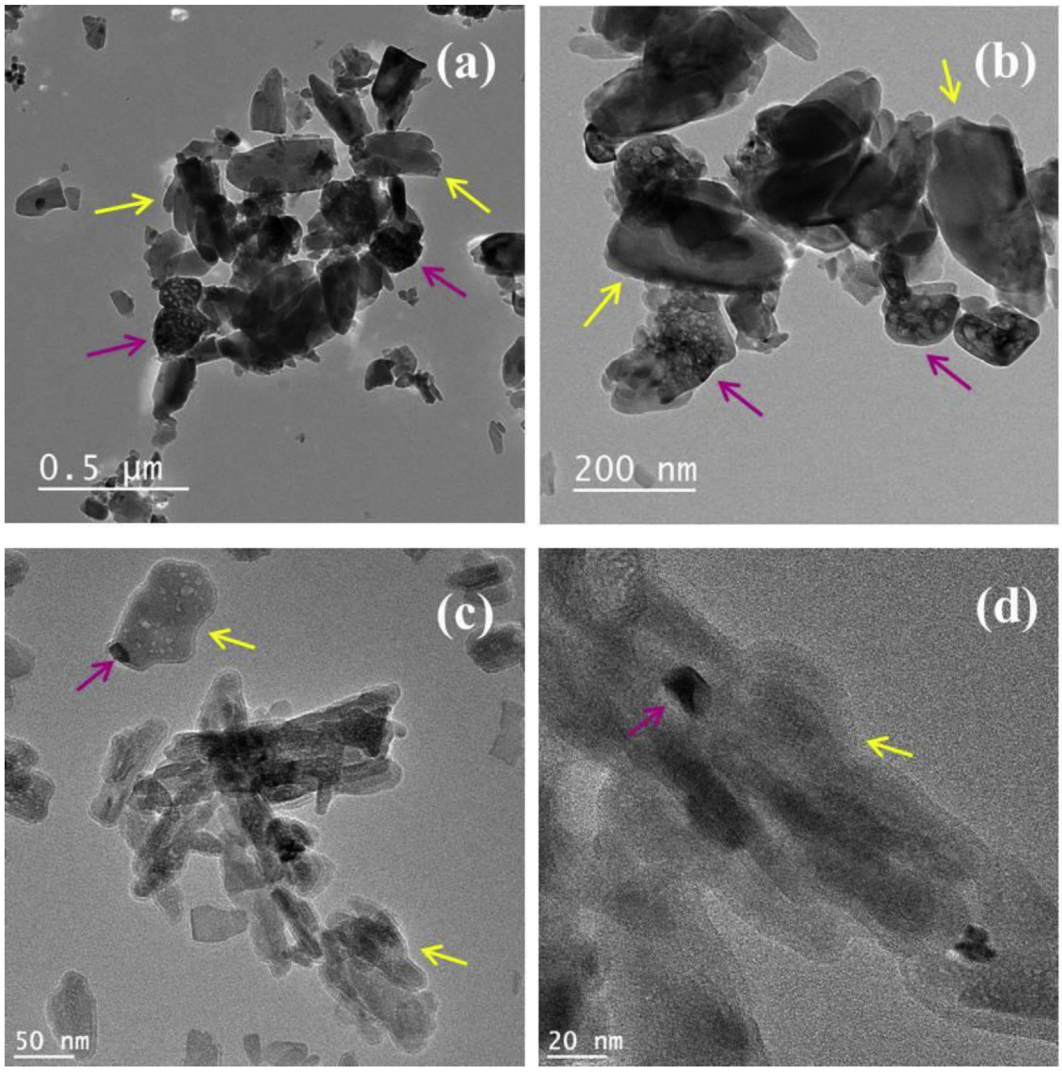

Fig. 4 – Examples of TEM images of calcined catalysts: (a) and (b) Ni/Ca-HA1, (c) and (d) Ni/Ca-HA2 catalysts; pink arrow: nickel particles, yellow arrow: hydroxyapatite particles. (For interpretation of the references to colour in this figure legend, the reader is referred to the Web version of this article.)

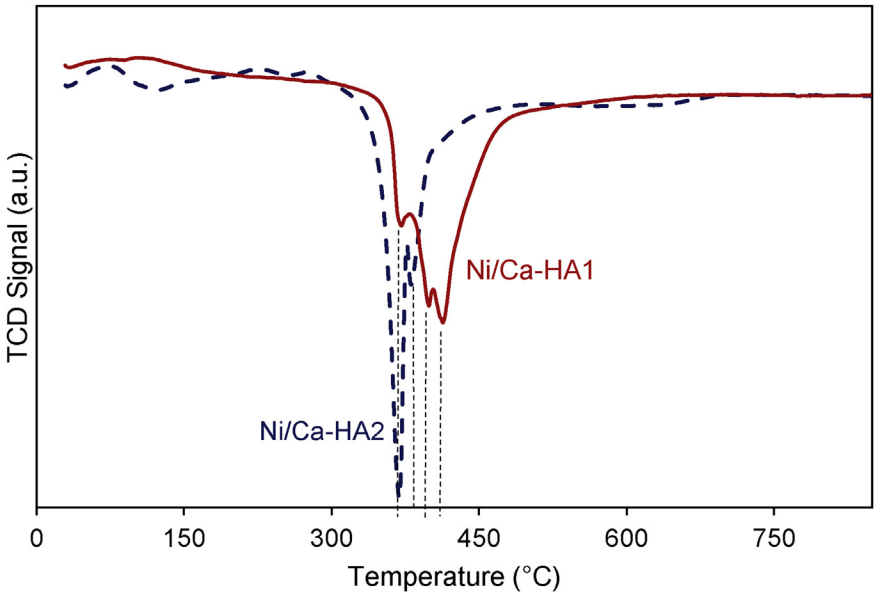

Fig. 5 – TPR of Ni/Ca-HA1 and Ni/Ca-HA2 catalysts.

peaks were found at 368 and 374 °C. These peaks were explained by the reduction of nickel oxide under H_2 flux [38,39]. Previous studies showed that the reduction of pure NiO usually follows the following steps: NiO → $Ni^{\gamma+}$ → Ni°, which take place at around 425 and 500 °C [40,41]. So, the reduction of nickel oxide particles of both catalysts of the present study happened in the temperature range lower than 450 °C. This indicates weak interaction between nickel particles and Ca-HA support. Furthermore, the sharpness of the reduction peaks obtained with Ni/Ca-HA2 could be also related to the high homogeneity of nickel particles. On the other hand, the broad peaks of Ni/Ca-HA1 could be due to its large and variable particle size.

The reduction of nickel species incorporated into the support structure usually occurs at temperatures higher than 600 °C [27,42,43]. So TPR results indicate that Ni^{2+} ions incorporated into the apatitic structure were negligible. This confirmed the XRD results presented above wherein any Ni-exchange-hydroxyapatite structure was detected. Probably, the incipient wetness impregnation conditions (no water excess) were not favorable for the ion exchange between apatitic Ca^{2+} and free Ni^{2+}. We note also that the ion exchange capacity of hydroxyapatite with Ni^{2+} is low (46 mg g^{-1}) [44] compared to other metals such as Pb^{2+} (1226 mg g^{-1}) [45] or Zn^{2+} (120 mg g^{-1}) [20].

Catalytic results

Influence of reaction temperature

The reaction temperature is one of the most important process parameters that can be controlled to ensure high conversion rates as well as to control carbon deposition (Supplementary material, Fig. S2) [5,12]. Hence, the effect of reaction temperature on the catalytic performance of the catalysts without thermal treatment (Ni/Ca-HA1 and Ni/Ca-HA2) was investigated in this work and the results are shown in Figs. 6 and 7, respectively. The total pressure was 1.6 bar, explained by fine particles of the catalyst bed causing pressure drop.

Ni/Ca-HA1 catalyst (Fig. 6) was active from 500 °C. As expected, the conversion of CH_4 and CO_2 as well as the selectivity to CO and H_2 increased with the increase of reaction temperature, as predicted by the thermodynamic calculation (Fig. S3). At 500 °C, CH_4 conversion was slightly higher than CO_2 conversion, suggesting that the catalytic methane cracking reaction (Eq. (4)) occurred to a large extent. Similar results were reported by several dry reforming of methane studies, in which the authors report the occurrence of methane decomposition up to 700 °C [11]. At 600 °C, the conversion of CH_4 and CO_2 were similar, which indicates the equilibrium between DRM and side reactions. At 700 °C, CO_2 conversion was slightly higher than CH_4 conversion. This might be related to the consumption of coke ($C_{(s)}$) by CO_2 (Eq. (3)) as well as to the RWGS (Eq. (2)). From 500 to 700 °C, the selectivity in H_2 was always higher than that in CO, as previously calculated by the thermodynamic study (Fig. S3). Moreover, at 700 °C, methane cracking is thermodynamically favored contrarily to the Boudouard reaction, which is reported to have its higher limit at 700 °C. These findings are in agreement with the thermodynamic calculations (Supplementary material) as well as with the thermodynamic studies reported in the literature [5,11,37].

Under similar conditions, Ni/Ca-HA2 catalyst was only active at 700 °C (Fig. 7). High reactants conversion and high selectivity in CO and H_2 were obtained with this catalyst at 700 °C. Consequently, the selectivity into H_2O and $C_{(s)}$ was relatively low at this temperature. The reason for the difference in the catalytic performance between the two catalysts might be related to the lower reducibility of the nickel particles present in the Ni/Ca-HA2 catalyst. The active phase for the dry reforming reaction is the metallic nickel (Ni^0). Hence, the initial nickel oxide particles have to be reduced to metallic

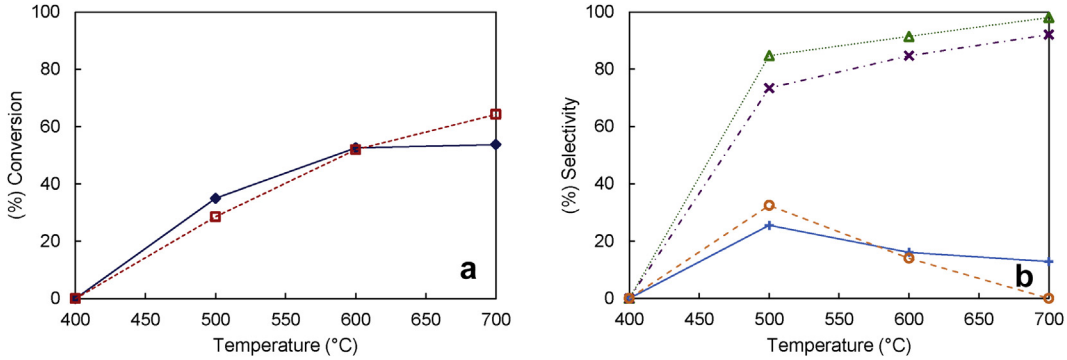

Fig. 6 – Influence of reaction temperature on (a) reactants conversion and (b) products selectivity for Ni/Ca-HA1 catalyst; ♦ CH_4, □ CO_2, ▲ H_2, x CO, + H_2O, ○ $C_{(s)}$. Other conditions: total pressure 1.6 bar, WHSV 15.9 L h^{-1} g_{cat}^{-1}.

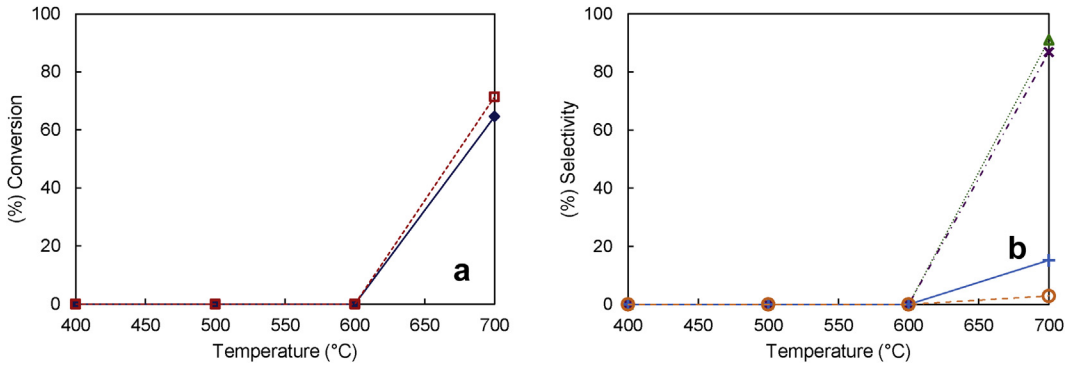

Fig. 7 – Influence of reaction temperature on (a) reactants conversion and (b) products selectivity for Ni/Ca-HA2 catalyst; ♦ CH_4, □ CO_2, ▲ H_2, x CO, + H_2O, ○ $C_{(s)}$. Other conditions: total pressure 1.6 bar, WHSV 15.9 L h^{-1} g_{cat}^{-1}.

nickel so that the catalyst can be actually active during the reaction [40,41]. However, depending on factors, such as metal-support interaction, for example, higher temperatures might be required to reduce the nickel particles, explaining why the Ni/Ca-HA2 catalyst was active only at 700 °C [5,37,46].

At 700 °C and 1.6 bar, the comparison of the reactants conversion showed that Ni/Ca-HA2 (Fig. 7) was more active than Ni/Ca-HA1 (Fig. 6). In fact, Ca-HA2 support had higher density of basic sites than Ca-HA1 support (Table 1), which favored the adsorption of CO_2 during DRM reaction. Moreover, Ni particles were smaller in Ni/Ca-HA2 than in Ni/Ca-HA1 (Fig. 4), leading to a higher dispersion of Ni in Ni/Ca-HA2.

As partial conclusion, the reaction temperature of 700 °C seemed to be the best choice for studying hydroxyapatite-based catalysts in DRM reaction, since it was the lowest temperature required to reach considerable reactants conversion and to highly limit the formation of byproducts. Ni/Ca-HA2 was more active than Ni/Ca-HA1 at 700 °C.

Influence of reaction pressure

Low pressures are required to attain high conversions and avoid carbon deposition (Supplementary material, Fig. S3). However, most of the processes for syngas conversion are usually performed at high pressures, such as Fischer-Tropsch synthesis, which requires about 20–25 bars [47–49]. Hence, syngas can be produced under pressure OR compressed after production. However, compressing hot syngas with high CO amount can be quite challenging and more energy-intensive than the first option [50]. So, the objective of this section was to investigate the influence of the reaction pressure on the syngas production and on the catalyst stability.

The effect of the total pressure on the catalytic performance of Ni/Ca-HA1 and Ni/Ca-HA2 catalysts at 700 °C is shown in Figs. 8 and 9, respectively.

High conversion of CH_4 and CO_2 (≈60–70%) was obtained with Ni/Ca-HA1 (Fig. 8) at the total pressure close to the atmospheric pressure. Then, it slightly decreased to around 50% when the total pressure increased to 25 bar, which was in accordance with the thermodynamic calculations (Fig. S3). The selectivity into H_2 and CO was initially very high (≈90–100%). However, they drastically decreased when increasing the total pressure, explained by the formation of coke and water by Boudouard and inverse carbon gasification reactions (Eqs. (3) and (5)). Particularly, the selectivity in coke was very high at 25 bar (close to 50%).

The total pressure had similar impacts on the catalytic activity of Ni/Ca-HA2 catalyst (Fig. 9) compared to Ni/Ca-HA1 catalyst (Fig. 8). The conversion of CH_4 and CO_2 drastically decreased from around 80% at 1.6 bar to around 45–50% at 25 bar. In parallel, H_2 and CO selectivity decreased from around 80–95% at 1.6 bar to around 60% above 15 bar. This decrease in the selectivity into CO and H_2 was also explained

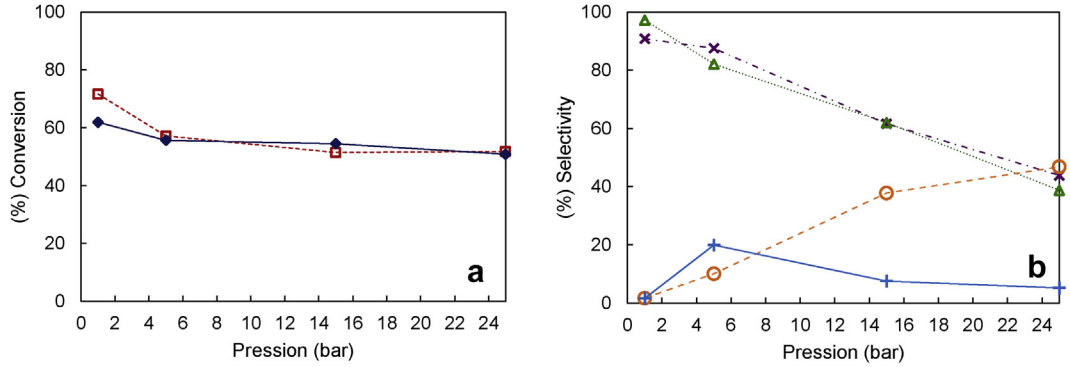

Fig. 8 – Influence of reaction pressure on (a) conversion and on (b) selectivity in DRM reaction using Ni/Ca-HA1 catalyst; ♦ CH_4, □ CO_2, ▲ H_2, x CO, + H_2O, ○ $C_{(s)}$. Other conditions: temperature 700 °C, WHSV 15.9 L h^{-1} g_{cat}^{-1}.

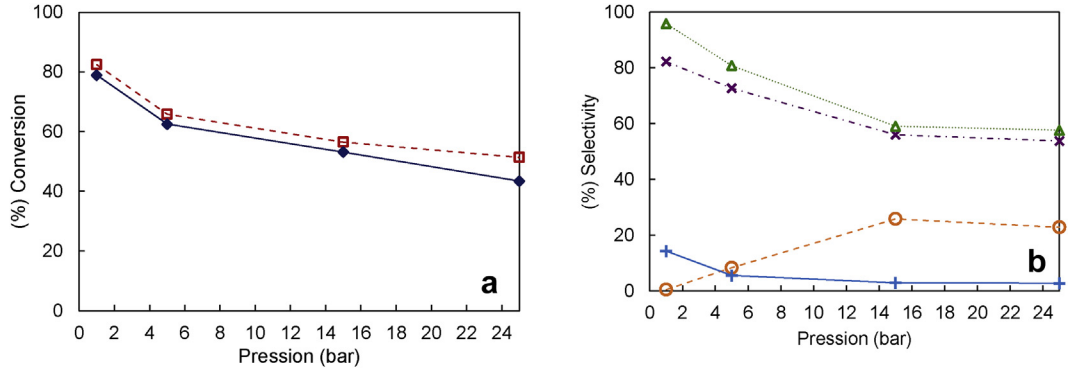

Fig. 9 – Influence of reaction pressure on (a) conversion and on (b) selectivity in DRM reaction using Ni/Ca-HA2 catalyst; ♦ CH_4, □ CO_2, ▲ H_2, x CO, + H_2O, ○ $C_{(s)}$. Other conditions: temperature 700 °C, WHSV 15.9 L h^{-1} g_{cat}^{-1}.

by the increase in the formation of water and coke as byproducts at high total pressures.

Similar conclusions were obtained by Jafarbegloo et al. [51] on the study of the impact of the total pressure. So for DRM, working closely to the standard atmospheric pressure is mandatory for keeping high reactants conversion and limiting the formation of byproducts.

Influence of catalyst pretreatment

Pretreatment before reaction is a key factor for the formation of the active metal sites, in this case metallic nickel (Ni^0). This parameter also influences the shape and size of nickel particles as well as the metal-support interaction that will later influence the catalytic performance of the catalysts [52,53]. In this work, the catalytic performance of the dried catalyst was compared to that of the *in situ* reduced catalyst. The pretreatment was performed at 700 °C for 1 h under 4%H_2/N_2 flow. The results are presented in Figs. 10 and 11.

The dried Ni/Ca-HA1 catalyst (Fig. 10) had around 60 and 70% of CH_4 and CO_2 conversion, respectively, during 7 h of time-on-stream (TOS). H_2 selectivity initially reached 98% and decreased to around 95% and CO selectivity was kept at 90% during the test. As consequence of high syngas selectivity, low H_2O and $C_{(s)}$ selectivity was observed. On the other hand, the initial conversion of CH_4 and CO_2 reached around 80% with the *in situ* reduced catalyst. Then, it decreased to 60–70% during the reaction. H_2 selectivity decreased from 95% to around 80%, while CO selectivity showed only a slight decrease from 100% to around 95% during the test. As for the catalyst without *in situ* reduction, very low H_2O and $C_{(s)}$ selectivity was observed. The better catalytic performance obtained with the reduced catalyst at the beginning of the experiment might be related to the reduction in a higher extent of the nickel particles prior to the DRM, generating the active phase Ni^0 that will convert the reactants from the beginning of the DRM step. The atmosphere present during the DRM might not be enough to completely reduce the nickel oxide particles, especially those with stronger metal-support interaction.

Fig. 11 shows the results obtained with Ni/Ca-HA2 catalyst. The initial conversion of CH_4 and CO_2 reached around 80%, which decreased to 60–70% during the reaction. H_2 selectivity was initially around 100% and decreased to 90%. CO selectivity was stable around 90% during the reaction. Conversely, the *in situ* reduced catalyst presented stable CH_4 and CO_2 conversion at around 80% during the test. The selectivity in both H_2 and CO was stable at around 90%. In all cases, H_2O and $C_{(s)}$ were formed at low amounts (selectivity < 10%). Similarly to the results presented in Fig. 10, the pretreated catalyst presented better catalytic performance than the catalyst without pretreatment.

As partial conclusion, the reduction step prior to the reaction (pretreatment) reduced more effectively the nickel oxide particles in both catalysts, being able to reduce nickel

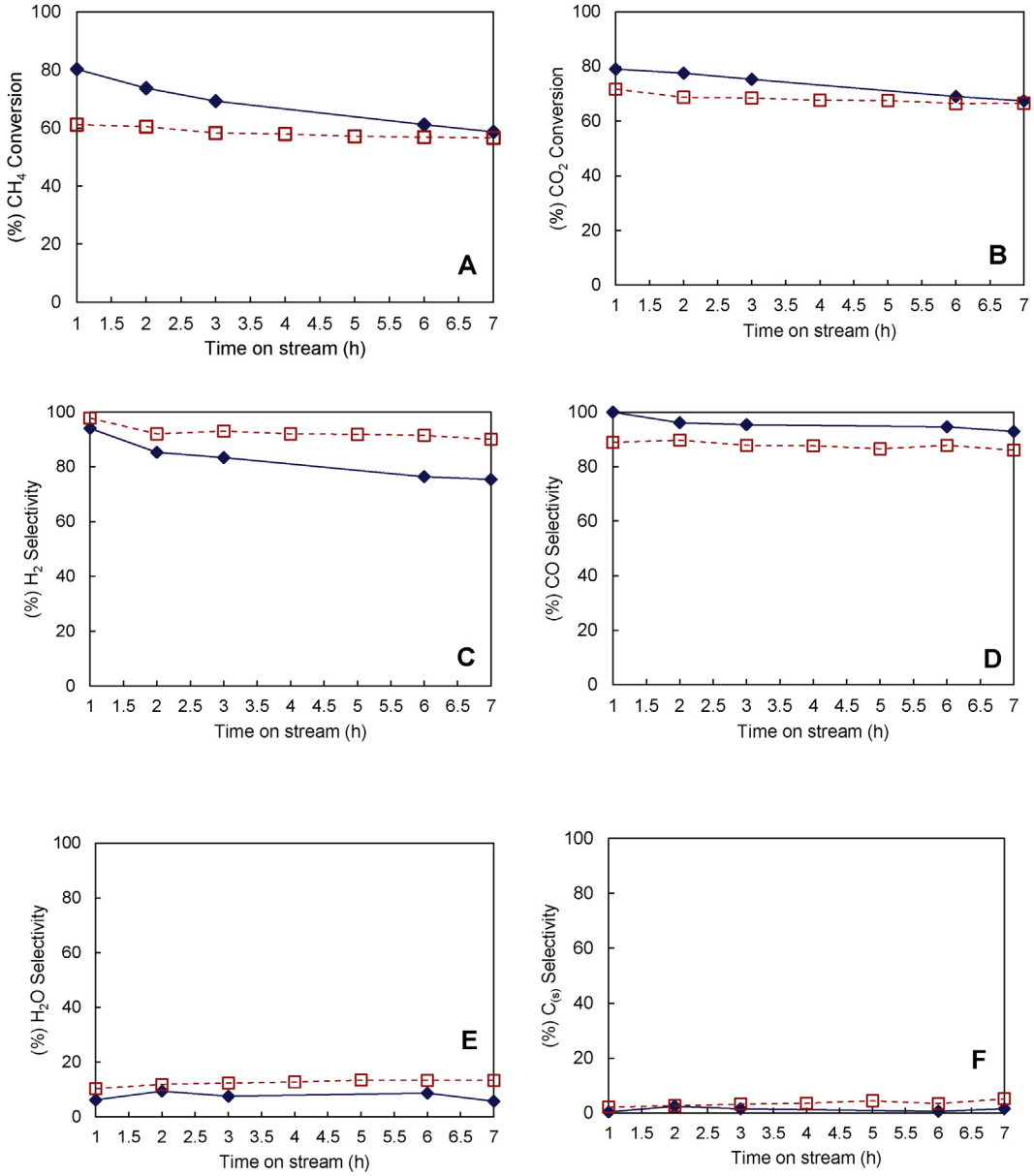

Fig. 10 – Catalytic performance of Ni/Ca-HA1 catalyst pretreated by (♦) *in situ* reduction, and (□) only drying. (A) CH_4 conversion, (B) CO_2 conversion, (C) H_2 selectivity, (D) CO selectivity, (E) H_2O selectivity, (F) $C_{(s)}$ selectivity. Other conditions: temperature 700 °C, total pressure 1.6 bar, WHSV 15.9 L h^{-1} g_{cat}^{-1}.

particles with strong metal-support interaction that could not be reduced during the reaction. Furthermore, among different catalysts tested, *in situ* reduced Ni/Ca-HA2 catalyst presented the best catalytic performance. This catalyst was not only active, but also stable after an initial slight deactivation (Fig. 11). This can be explained by large specific surface area, the presence of mesoporosity of Ca-HA2 support, which resulted in the high dispersion of nickel, as well as by high density of basic sites of this support (Fig. 2), which favored CO_2 adsorption during DRM reaction.

Influence of the thermal treatment of Ca-HA support

DRM process needs high temperatures in order to obtain high syngas yield and avoid carbon deposition, as presented previously (Fig. S3). However, thermal treatment of the catalyst at high temperature could also lead to catalyst deactivation [41,54,55]. To anticipate this phenomenon during the catalytic reaction, we performed a thermal treatment of the support prior to nickel deposition. Ca-HA1 and Ca-HA2 supports were heated under air atmosphere at 1000 °C for 5 h, which decreased the specific surface area of both supports to <3 m^2/g. This modification has been explained elsewhere [48]. Figs. 12 and 14 show the impact of the thermal treatment step on the catalytic property of the catalysts.

Ni/Ca-HA1 catalyst (support without thermal treatment, Fig. 12, blue curves) had good catalytic performance, showing high initial conversion of CO_2 and CH_4 at around 80%, which decreased to around 60–70% during the test. H_2 selectivity was initially high around 90% and decreased to 75%. Similarly, CO selectivity decreased from 100% to 93% during the test.

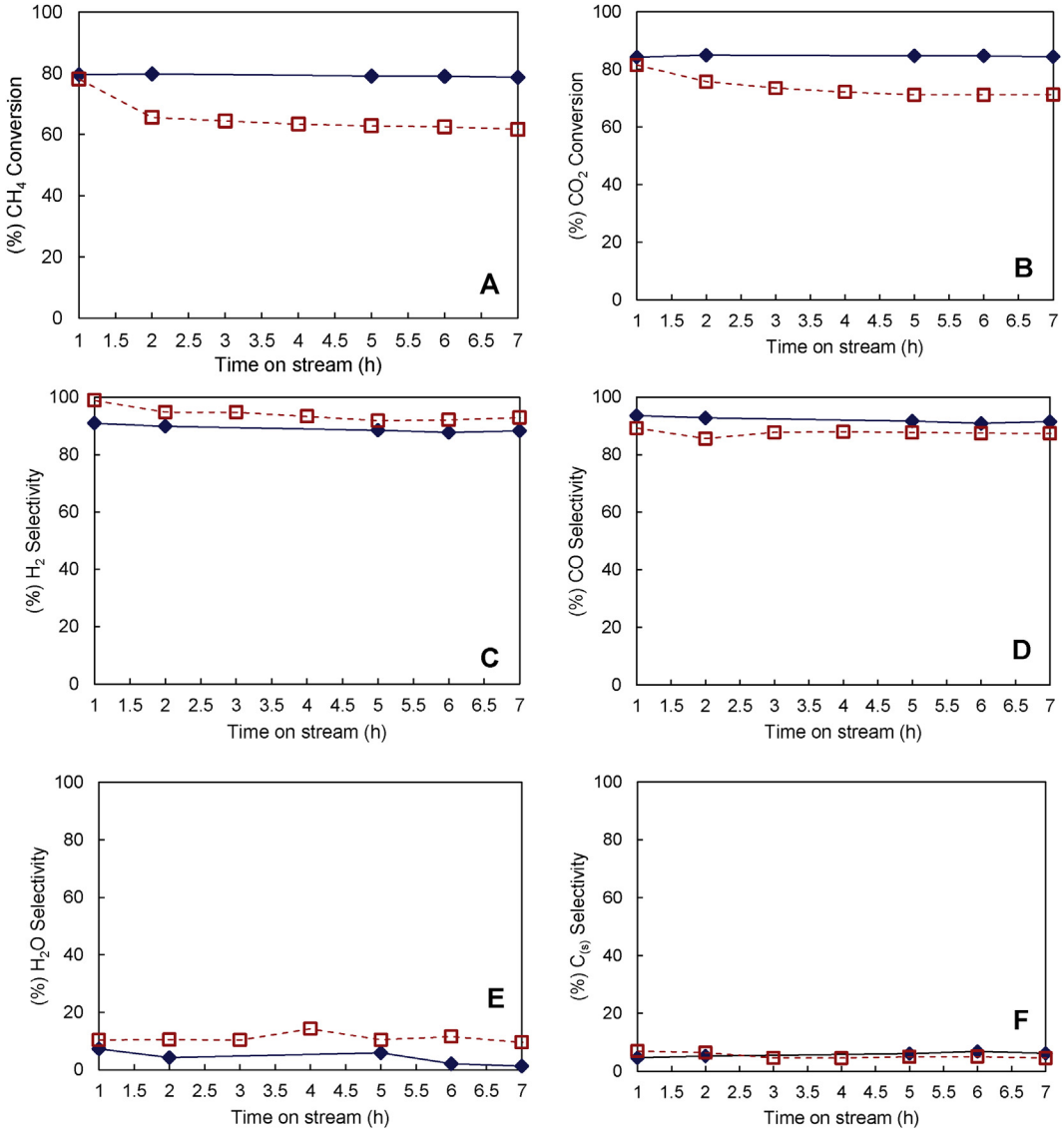

Fig. 11 – Catalytic performance of Ni/Ca-HA2 catalyst pretreated by (♦) *in situ* reduction, and (□) only drying. (A) CH_4 conversion, (B) CO_2 conversion, (C) H_2 selectivity, (D) CO selectivity, (E) H_2O selectivity, (F) $C_{(s)}$ selectivity. Other conditions: temperature 700 °C, total pressure 1.6 bar, WHSV 15.9 L h^{-1} g_{cat}^{-1}.

Byproducts selectivity was very low during the test (<10% for H_2O and <2% for $C_{(s)}$). On the other hand, Ni/Ca-HA1_S catalyst prepared with the thermal treated support (Fig. 12, red curves) had low initial conversion of CH_4 and CO_2 (around 30–40%) under the same conditions. This drastically decreased to 15–20% after 7 h of TOS. H_2 selectivity decreased from 45 to 10% while CO selectivity decreased from 70 to around 40%. Consequently, the selectivity into byproducts was high: 30–50% for H_2O and 20–50% for $C_{(s)}$. The high $C_{(s)}$ selectivity indicates the occurrence of carbon-forming reactions (Eqs. (3) and (4)) by this catalyst.

High $C_{(s)}$ selectivity is usually due to large nickel particles [56]. However, nickel particle sizes of both catalysts were similar (Fig. 13). TEM analysis (Fig. 4a,b) showed nickel particle size around 100–200 nm for Ni/Ca-HA1. We suppose that the low catalytic activity of Ni/Ca-HA1_S catalyst could be due to the reduction of the specific surface area after thermal treatment (S_{BET} < 3 m^2/g); the change in the acid-basic property because of the dehydration of hydroxide groups of the apatitic structure; or the change in metal-support interaction. Further characterization is needed to evidence this catalytic result.

In the case of the support Ca-HA2, the thermal treatment step (calcination at 1000 °C for 5 h) had much less impact on the performance of the prepared catalysts. The initial conversion of both CH_4 and CO_2 was slightly decreased by the thermal treatment: from 80 to 70% for CH_4 and from 90 to 77% for CO_2. During 7 h of TOS, Ni/Ca-HA2 catalyst (support without thermal treatment, Fig. 14, blue curves) did not practically change its catalytic performance. On the other hand, Ni/Ca-HA2_S catalyst (support thermally treated, Fig. 14, red curves) had a slight deactivation with 65% of CH_4 and conversion 70% of CO_2 conversion at 7 h of TOS.

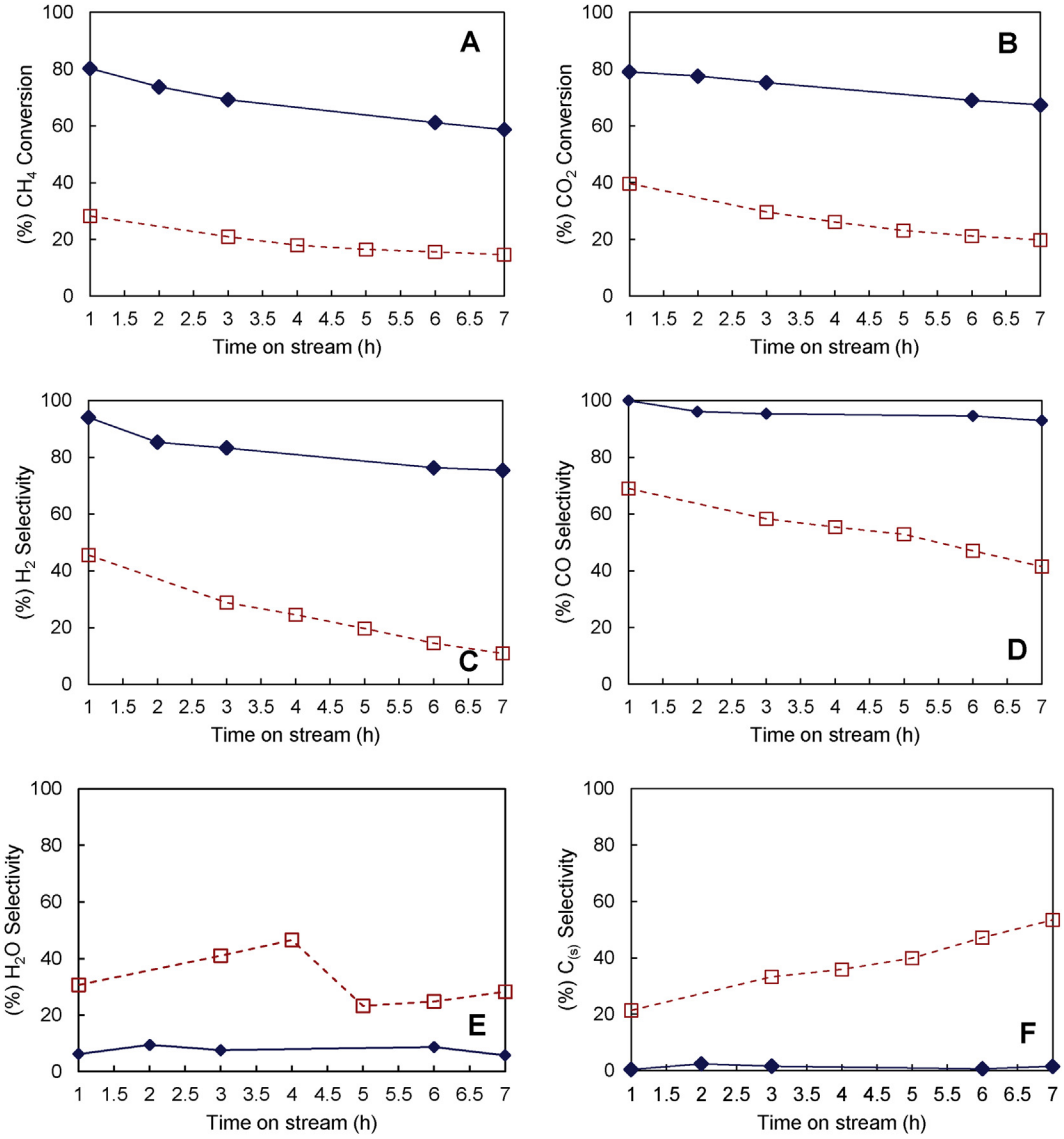

Fig. 12 – Catalytic performance of (♦) Ni/Ca-HA1 catalyst prepared with support without thermal treatment, and (□) Ni/Ca-HA1_S prepared with thermally treated support. (A) CH_4 conversion, (B) CO_2 conversion, (C) H_2 selectivity, (D) CO selectivity, (E) H_2O selectivity, (F) $C_{(s)}$ selectivity. Other conditions: temperature 700 °C, total pressure 1.6 bar, WHSV 15.9 L h^{-1} g_{cat}^{-1}.

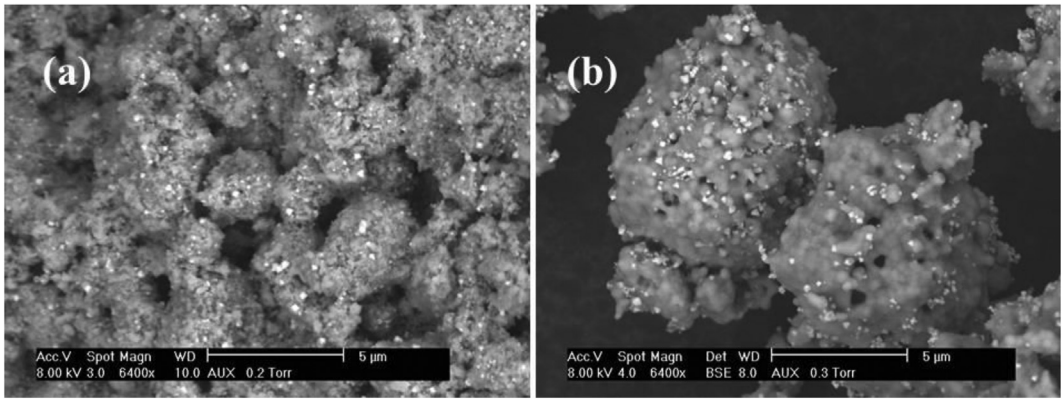

Fig. 13 – SEM images of Ca-HA1 based catalysts prepared with (a) initial support and (b) support thermally treated.

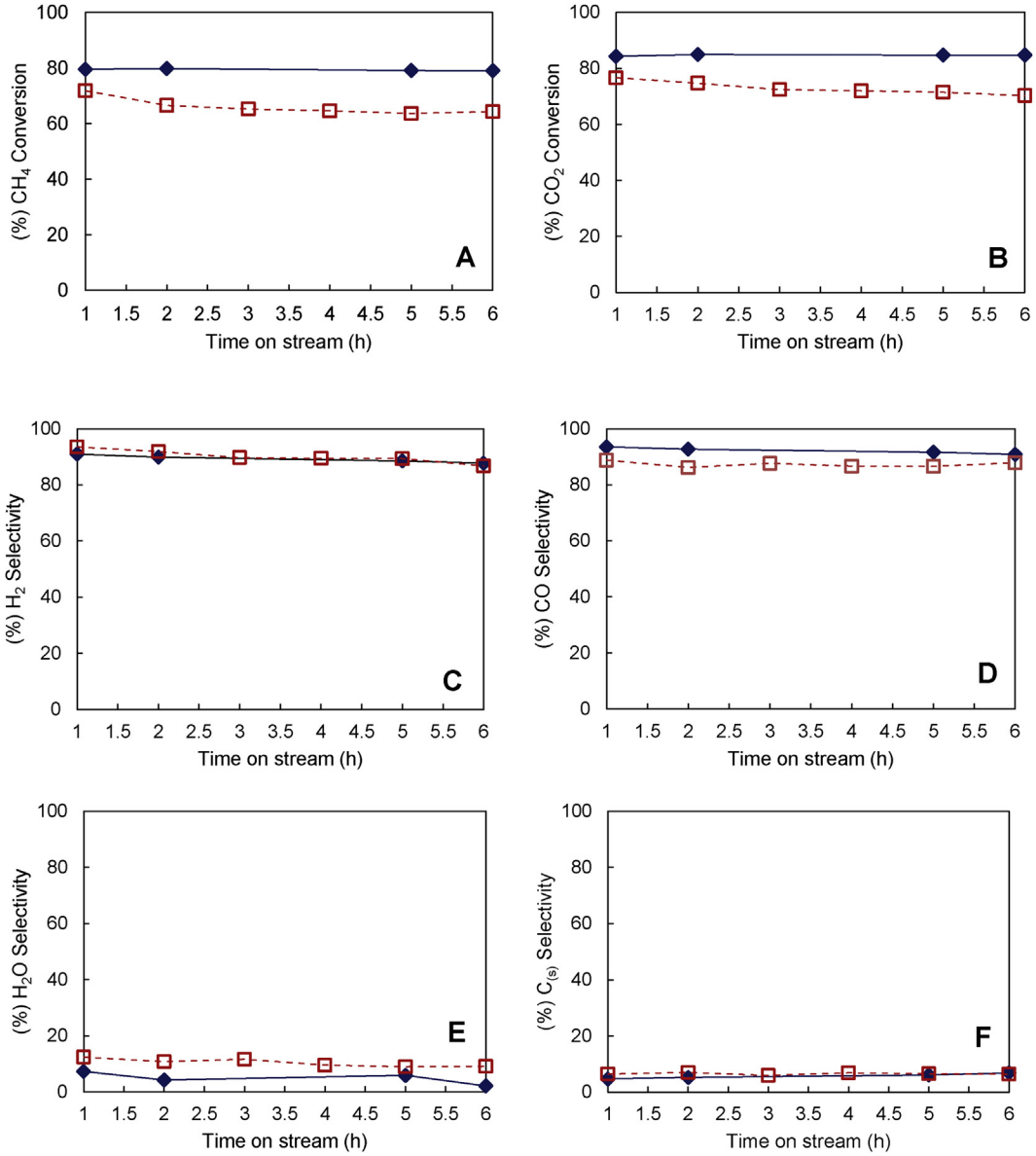

Fig. 14 – Catalytic performance of (♦) Ni/Ca-HA2 catalyst prepared with support without thermal treatment, and (□) Ni/Ca-HA2_S prepared with support thermally treated. (A) CH_4 conversion, (B) CO_2 conversion, (C) H_2 selectivity, (D) CO selectivity, (E) H_2O selectivity, (F) $C_{(s)}$ selectivity. Other conditions: temperature 700 °C, total pressure 1.6 bar, WHSV 15.9 L h^{-1} g_{cat}^{-1}.

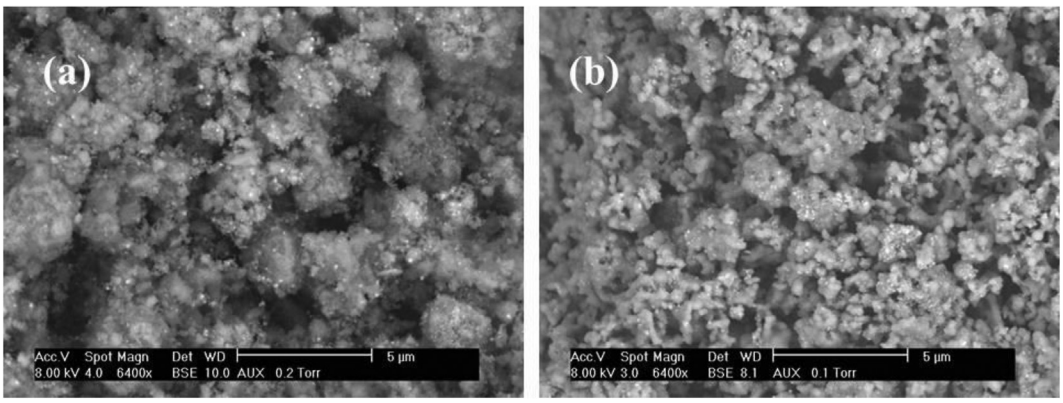

Fig. 15 – SEM images of Ca-HA2 based catalysts prepared with (a) initial support and (b) support thermally treated.

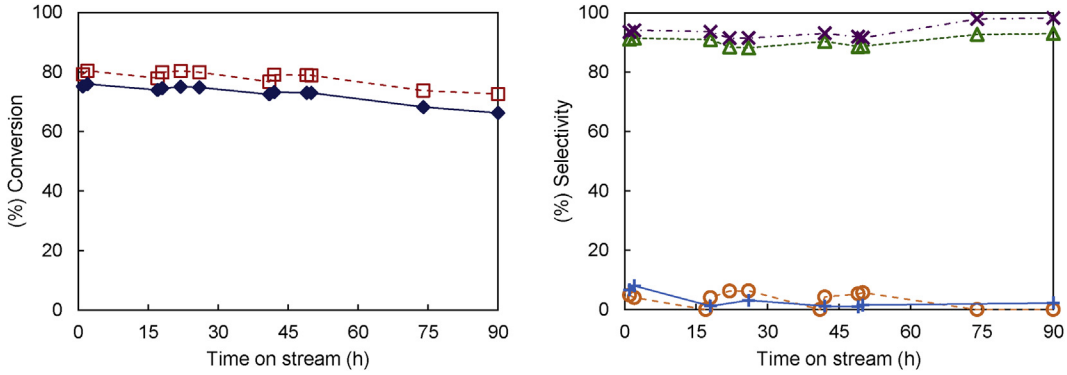

Fig. 16 – Catalytic performance of *in situ* reduced Ni/Ca-HA2 catalyst during 90 h of TOS; ♦ CH_4, □ CO_2, ▲ H_2, x CO, + H_2O, ○ $C_{(s)}$. Reaction conditions: temperature 700 °C, total pressure 1.6 bar, WHSV 15.9 L h^{-1} g_{cat}^{-1}.

Both catalysts with and without thermal treatment showed the similar selectivity in H_2 and CO which reached around 90%. Consequently, the selectivity into H_2O and $C_{(s)}$ was low and did not exceed 10% during the test.

Fig. 15 shows that the calcination step led to the densification of Ca-HA2 support. However, the size of nickel particles was similar to each other (10–20 nm for Ni/Ca-HA2 as shown in Fig. 4c,d). Nickel particles were well distributed on the surface of both the supports. This explains the similarity of the catalytic results in Fig. 14. The good performance of these catalysts could be linked with the nanometric size of nickel particles. In fact, there is a consensus that small nickel particles may prevent carbon deposition and catalyst deactivation [6,10,50–54]. The high basicity of Ca-HA2 was also favorable for DRM reaction.

For the thermally treated Ca-HA2 support, despite its low specific surface area (S_{BET} < 3 m^2/g), nickel particles of 10–20 nm were formed, which was not the case for the thermally treated Ca-HA1 support. Further characterization is needed to identify factors which control the formation of nickel particles on hydroxyapatite surface.

Stability study

The *in situ* reduced Ni/Ca-HA2 catalyst showed the highest performance during 7 h of TOS at 700 °C, and 1.6 bar. However, longer reaction time is needed to better evaluate its catalytic behavior. Fig. 16 shows the results obtained for long reaction time with this catalyst.

Ni/Ca-HA2 catalyst showed high initial CH_4 conversion (78%) which slowly decreased to 66% during 90 h of TOS. Similarly, CO_2 conversion decreased slowly from 84% to 73%. CO_2 conversion was higher compared to CH_4 conversion, which could be explained by the occurrence of RWGS (Eq. (2)). Along the test, H_2 and CO were the two main products with more than 90% of selectivity, while H_2O and $C_{(s)}$ were only formed at less than 10% of selectivity.

Fig. 17 shows TEM and SEM images of the spent catalyst recovered from the test in Fig. 16. The size of Ni particles was still found within 10–20 nm (Fig. 17a) after 90 h of test, indicating that the sintering of the nickel particles did not happen. The deactivation of the catalyst could be explained by coke deposition as illustrated in Fig. 17b. This deposition must decrease the availability of nickel particles, thus decreasing the catalytic activity of the catalyst.

Table 2 compares the results obtained in this study with some results reported in the literature on Ni-based catalysts in DRM reaction. Under comparable test conditions, our catalyst (Ni/Ca-HA2) presented similar catalytic performance than the catalysts prepared with the conventional metal oxides supports. But our Ni/Ca-HA2 catalyst was found to be thermally

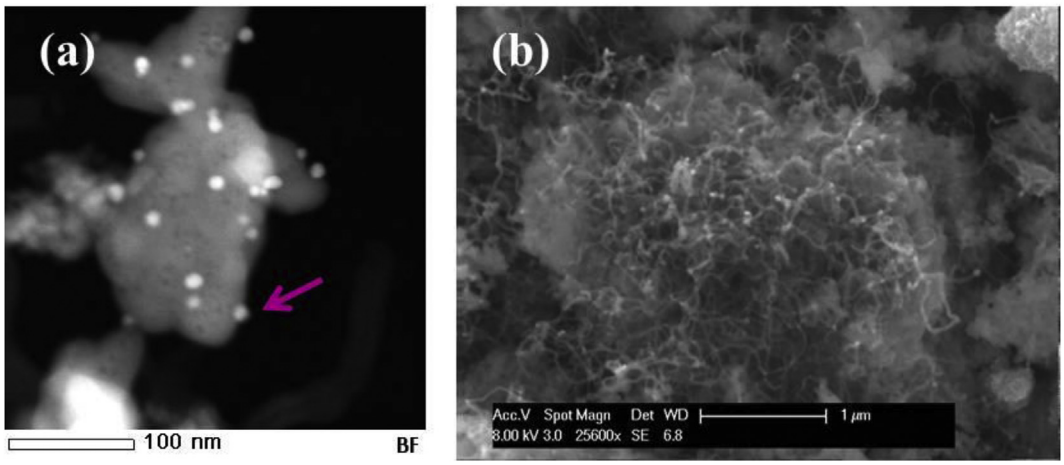

Fig. 17 – (a) TEM and (b) SEM images of spent Ni/Ca-HA2 catalyst after 90 h of TOS; Pink arrow: one Ni particle. (For interpretation of the references to colour in this figure legend, the reader is referred to the Web version of this article.)

Table 2 – Reactivity of Ni-based catalysts in DRM reaction at 700 °C and ambient pressure.

Catalyst	Metal content (wt.%)	Catalyst weight (mg)	CH_4/CO_2 conversion (%)	Time on stream (h)	Ref.
$NiLa_2O_3/ZrO_2$	Ni: 5	200	70/nd	50	[57]
Ni/Al_2O_3	Ni: 6.6	180	67/75	24	[58]
$Ni\text{-}Mg/Al_2O_3$	Ni: 5, Mg: 3	200	77/nd	22	[59]
Ni/CeO_2	Ni: 5	50	40-15/80-40	12	[60]
Ni/Ca-HA2	Ni: 5	300	78-66/84-73	90	This work

stable after a thermal treatment at 1000 °C. This is a crucial result to design an efficient catalyst for DRM reaction.

Conclusions

Two hydroxyapatites (Ca-HA1 and Ca-HA2) with different physico-chemical properties were doped with nickel by incipient wetness impregnation method and evaluated in DRM reaction. The influence of temperature, pressure, catalyst pretreatment and support thermal treatment on the catalytic properties was investigated. The catalytic activity and stability strongly depended on the nickel particle size, and on the reaction temperature and pressure. Ni/Ca-HA2 with nickel particle size of 10–20 nm was highly active and relatively stable for 90 h of test. The temperature of 700 °C seemed to be the best choice to get high reactants conversion while the pressure of 1.6 bar was mandatory for high syngas selectivity and low byproducts selectivity. These results match well with the thermodynamic calculation. The *in situ* reduction under H_2 improved the performance of the catalysts by completely activating nickel particles prior to the reaction. The thermal treatment by calcination under air atmosphere of the support before nickel deposition affected only slightly the catalytic behavior of Ni/Ca-HA2. This result is crucial to design a performing nickel catalyst for DRM reaction without further risk of thermal sintering.

Acknowledgment

The authors gratefully thank PRAYON and Association Nationale de la Recherche et de la Technologie (ANRT) for financial support, and colleagues at RAPSODEE lab for technical help.

Appendix A. Supplementary data

Supplementary data to this article can be found online at https://doi.org/10.1016/j.ijhydene.2019.08.068.

REFERENCES

[1] Alipour Moghadam Esfahani R, Osmieri L, Specchia S, Yusup S, Tavasoli A, Zamaniyan A. H2-rich syngas production through mixed residual biomass and HDPE waste via integrated catalytic gasification and tar cracking plus biochar upgrading. Chem Eng J 2017;308:578–87. https://doi.org/10.1016/j.cej.2016.09.049.

[2] Woolcock PJ, Brown RC. A review of cleaning technologies for biomass-derived syngas. Biomass Bioenergy 2013;52:54–84. https://doi.org/10.1016/j.biombioe.2013.02.036.

[3] Newnham J, Mantri K, Amin MH, Tardio J, Bhargava SK. Highly stable and active Ni-mesoporous alumina catalysts for dry reforming of methane. Int J Hydrogen Energy 2012;37:1454–64. https://doi.org/10.1016/j.ijhydene.2011.10.036.

[4] Rêgo de Vasconcelos B, Zhao L, Sharrock P, Nzihou A, Pham Minh D. Catalytic transformation of carbon dioxide and methane into syngas over ruthenium and platinum supported hydroxyapatites. Appl Surf Sci 2016;390:141–56. https://doi.org/10.1016/j.apsusc.2016.08.077.

[5] Usman M, Wan Daud WMA, Abbas HF. Dry reforming of methane: influence of process parameters—a review. Renew Sustain Energy Rev 2015;45:710–44. https://doi.org/10.1016/j.rser.2015.02.026.

[6] Farniaei M, Abbasi M, Rahnama H, Rahimpour MR, Shariati A. Syngas production in a novel methane dry reformer by utilizing of tri-reforming process for energy supplying: modeling and simulation. J Nat Gas Sci Eng 2014;20:132–46. https://doi.org/10.1016/j.jngse.2014.06.010.

[7] Wurzel T, Malcus S, Mleczko L. Reaction engineering investigations of CO reforming in a fuidized-bed reactor. Chem Eng Sci 2000;55:3955–66. https://doi.org/10.1016/S0009-2509(99)00444-3.

[8] Shang Z, Li S, Li L, Liu G, Liang X. Highly active and stable alumina supported nickel nanoparticle catalysts for dry reforming of methane. Appl Catal B Environ 2017;201:302–9. https://doi.org/10.1016/j.apcatb.2016.08.019.

[9] Rego de Vasconcelos B, Lavoie J-M. Is dry reforming the solution to reduce natural gas carbon footprint? Int J Energy Prod Manag 2018;3:44–56. https://doi.org/10.2495/EQ-V3-N1-44-56.

[10] Arora S, Prasad R. An overview on dry reforming of methane: strategies to reduce carbonaceous deactivation of catalysts. RSC Adv 2016;6:108668–88. https://doi.org/10.1039/c6ra20450c.

[11] Jang WJ, Shim JO, Kim HM, Yoo SY, Roh HS. A review on dry reforming of methane in aspect of catalytic properties. Catal Today 2019;324:15–26. https://doi.org/10.1016/j.cattod.2018.07.032.

[12] Muraza O, Galadima A. A review on coke management during dry reforming of methane. Int J Energy Res 2016;39:1196–216. https://doi.org/10.1002/er3295.

[13] Kim J-H, Suh DJ, Park T-J, Kim K-L. Effect of metal particle size on coking during CO2 reforming of CH4 over Ni–alumina aerogel catalysts. Appl Catal A Gen 2000;197:191–200. https://doi.org/10.1016/S0926-860X(99)00487-1.

[14] Frontera P, Macario A, Aloise A, Antonucci PL, Giordano G, Nagy JB. Effect of support surface on methane dry-reforming catalyst preparation. Catal Today 2013;218–219:18–29. https://doi.org/10.1016/j.cattod.2013.04.029.

[15] García-Diéguez M, Pieta IS, Herrera MC, Larrubia MA, Alemany LJ. Nanostructured Pt- and Ni-based catalysts for

CO2-reforming of methane. J Catal 2010;270:136–45. https://doi.org/10.1016/j.jcat.2009.12.010.
[16] Garcia-Vargas JM, Valverde JL, Dorado F, Sanchez P. Influence of the support on the catalytic behaviour of Ni catalysts for the dry reforming reaction and the tri-reforming process. J Mol Catal A Chem 2014;395:108–16. https://doi.org/10.1016/j.molcata.2014.08.019.
[17] Gac W, Derylo-Marczewska A, Pasieczna-Patkowska S, Popivnyak N, Zukocinski G. The influence of the preparation methods and pretreatment conditions on the properties of Ag-MCM-41 catalysts. J Mol Catal A Chem 2007;268:15–23. https://doi.org/10.1016/j.molcata.2006.12.002.
[18] Chen G, Shan R, Shi J, Liu C, Yan B. Biodiesel production from palm oil using active and stable K doped hydroxyapatite catalysts. Energy Convers Manag 2015;98:463–9. https://doi.org/10.1016/j.enconman.2015.04.012.
[19] Bailliez S, Nzihou A, Bèche E, Flamant G. Removal of lead (Pb) by hydroxyapatite sorbent. Process Saf Environ Prot 2004;82:175–80. https://doi.org/10.1205/095758204322972816.
[20] Sebei H, Pham Minh D, Nzihou A, Sharrock P. Sorption behavior of Zn(II) ions on synthetic apatitic calcium phosphates. Appl Surf Sci 2015;357:1958–66. https://doi.org/10.1016/j.apsusc.2015.09.158.
[21] Huang C, Ma Z, Xie P, Yue Y, Hua W, Gao Z. Hydroxyapatite-supported rhodium catalysts for N2O decomposition. J Mol Catal A Chem 2015;400:90–4. https://doi.org/10.1016/j.molcata.2015.02.011.
[22] Boukha Z, González-Prior J, de Rivas B, González-Velasco JR, López-Fonseca R, Gutiérrez-Ortiz JI. Synthesis, characterisation and behaviour of Co/hydroxyapatite catalysts in the oxidation of 1,2-dichloroethane. Appl Catal B Environ 2016;190:125–36. https://doi.org/10.1016/j.apcatb.2016.03.005.
[23] Bailliez S, Nzihou A. The kinetics of surface area reduction during isothermal sintering of hydroxyapatite adsorbent. Chem Eng J 2004;98:141–52. https://doi.org/10.1016/j.cej.2003.07.001.
[24] Venugopal A, Scurrell MS. Hydroxyapatite as a novel support for gold and ruthenium catalysts Behaviour in the water gas shift reaction. Appl Catal A Gen 2003;245:137–47. https://doi.org/10.1016/S0926-860X(02)00647-6.
[25] Bauer JE, Lewis GJ. Low coke formation catalysts and process for reforming and synthesis gas production. US 6544439 B1. 2003.
[26] Yaakob Z, Hakim L, Kumar M, Ismail M, Daud W. Hydroxyapatite supported Nickel catalyst for hydrogen production. Am J Sci Ind Res 2010;1:122–6. https://doi.org/10.5251/ajsir.2010.1.2.122.126.
[27] Boukha Z, Kacimi M, Pereira MFR, Faria JL, Figueiredo JL, Ziyad M. Methane dry reforming on Ni loaded hydroxyapatite and fluoroapatite. Appl Catal A Gen 2007;317:299–309. https://doi.org/10.1016/j.apcata.2006.10.029.
[28] Li X, Zhang D, Liu X, Shi L, Sun L. A tandem demetalization – desilication strategy to enhance the porosity of attapulgite for adsorption and catalysis. Chem Eng Sci 2016;141:184–94. https://doi.org/10.1016/j.ces.2015.11.011.
[29] Sing KSW, Everett DH, Haul RAW, Moscou L, Pierotti RA, Rouquerol J, et al. Reporting physisorption data for gas/solid systems. Handb. Heterog. Catal. Wiley-VCH Verlag GmbH & Co. KGaA; 2008. p. 1217–30. https://doi.org/10.1002/9783527610044.hetcat0065.
[30] Lowell S, Shields JE. Adsorption isotherms. Powder surf. Area porosity. Springer Netherlands; 1991. p. 11–3. https://doi.org/10.1007/978-94-015-7955-1_3.
[31] Sengupta S, Deo G. Modifying alumina with CaO or MgO in supported Ni and Ni–Co catalysts and its effect on dry reforming of CH4. J CO2 Util 2015;10:67–77. https://doi.org/10.1016/j.jcou.2015.04.003.
[32] Siahvashi A, Adesina AA. Synthesis gas production via propane dry (CO2) reforming: influence of potassium promotion on bimetallic Mo-Ni/Al2O3. Catal Today 2013;214:30–41. https://doi.org/10.1016/j.cattod.2012.12.005.
[33] Han SJ, Bang Y, Kwon HJ, Lee HC, Hiremath V, Song IK, et al. Elevated temperature CO2 capture on nano-structured MgO-Al2O3 aerogel: effect of Mg/Al molar ratio. Chem Eng J 2014;242:357–63. https://doi.org/10.1016/j.cej.2013.12.092.
[34] Navajas A, Campo I, Arzamendi G, Hernandez WY, Bobadilla LF, Centeno MA, et al. Synthesis of biodiesel from the methanolysis of sunflower oil using PURAL Mg-Al hydrotalcites as catalyst precursors. Appl Catal B Environ 2010;100:299–309. https://doi.org/10.1016/j.apcatb.2010.08.006.
[35] Stošić D, Bennici S, Sirotin S, Calais C, Couturier JL, Dubois JL, et al. Glycerol dehydration over calcium phosphate catalysts: effect of acidic-basic features on catalytic performance. Appl Catal A Gen 2012;447–448:124–34. https://doi.org/10.1016/j.apcata.2012.09.029.
[36] Aramouni NAK, Touma JG, Tarboush BA, Zeaiter J, Ahmad MN. Catalyst design for dry reforming of methane: analysis review. Renew Sustain Energy Rev 2018;82:2570–85. https://doi.org/10.1016/j.rser.2017.09.076.
[37] Pakhare D, Spivey J. A review of dry (CO2) reforming of methane over noble metal catalysts. Chem Soc Rev 2014;43:7813–37. https://doi.org/10.1039/c3cs60395d.
[38] Ahmed W, El-Din MRN, Aboul-Enein AA, Awadallah AE. Effect of textural properties of alumina support on the catalytic performance of Ni/Al2O3 catalysts for hydrogen production via methane decomposition. J Nat Gas Sci Eng 2015;25:359–66. https://doi.org/10.1016/j.jngse.2015.05.015.
[39] Wu P, Li X, Ji S, Lang B, Habimana F, Li C. Steam reforming of methane to hydrogen over Ni-based metal monolith catalysts. Catal Today 2009;146:82–6. https://doi.org/10.1016/j.cattod.2009.01.031.
[40] Xu S, Yan X, Wang X. Catalytic performances of NiO–CeO2 for the reforming of methane with CO2 and O2. Fuel 2006;85:2243–7. https://doi.org/10.1016/j.fuel.2006.03.022.
[41] Ay H, Üner D. Dry reforming of methane over CeO2 supported Ni, Co and Ni–Co catalysts. Appl Catal B Environ 2015;179:128–38. https://doi.org/10.1016/j.apcatb.2015.05.013.
[42] Gálvez ME, Albarazi A, Da Costa P. Enhanced catalytic stability through non-conventional synthesis of Ni/SBA-15 for methane dry reforming at low temperatures. Appl Catal A Gen 2015;504:143–50. https://doi.org/10.1016/j.apcata.2014.10.026.
[43] Goula MA, Charisiou ND, Papageridis KN, Delimitis A, Pachatouridou E, Iliopoulou EF. Nickel on alumina catalysts for the production of hydrogen rich mixtures via the biogas dry reforming reaction: influence of the synthesis method. Int J Hydrogen Energy 2015;40:9183–200. https://doi.org/10.1016/j.ijhydene.2015.05.129.
[44] Mobasherpour I, Salahi E, Pazouki M. Removal of nickel (II) from aqueous solutions by using nano-crystalline calcium hydroxyapatite. J Saudi Chem Soc 2011;15:105–12. https://doi.org/10.1016/j.jscs.2010.06.003.
[45] Pham Minh D, Tran ND, Nzihou A, Sharrock P. Calcium phosphate based materials starting from calcium carbonate and orthophosphoric acid for the removal of lead(II) from an aqueous solution. Chem Eng J 2014;243:280–8. https://doi.org/10.1016/j.cej.2014.01.032.
[46] Wang F, Xu L, Zhang J, Zhao Y, Li H, Li HX, et al. Tuning the metal-support interaction in catalysts for highly efficient methane dry reforming reaction. Appl Catal B Environ

2016;180:511–20. https://doi.org/10.1016/j.apcatb.2015.07.001.
[47] Dry ME. The Fischer – Tropsch process 1950 – 2000. Catal Today 2002;71:227–41. https://doi.org/10.1016/S0920-5861(01)00453-9.
[48] Selvatico D, Lanzini A, Santarelli M. Low temperature Fischer-Tropsch fuels from syngas: kinetic modeling and process simulation of different plant configurations. Fuel 2016;186:544–60. https://doi.org/10.1016/j.fuel.2016.08.093.
[49] Okoye-Chine CG, Moyo M, Liu X, Hildebrandt D. A critical review of the impact of water on cobalt-based catalysts in Fischer-Tropsch synthesis. Fuel Process Technol 2019;192:105–29. https://doi.org/10.1016/j.fuproc.2019.04.006.
[50] Chein RY, Chen YC, Yu CT, Chung JN. Thermodynamic analysis of dry reforming of CH4 with CO2 at high pressures. J Nat Gas Sci Eng 2015;26:617–29. https://doi.org/10.1016/j.jngse.2015.07.001.
[51] Jafarbegloo M, Tarlani A, Mesbah AW, Sahebdelfar S. Thermodynamic analysis of carbon dioxide reforming of methane and its practical relevance. Int J Hydrogen Energy 2015;40:2445–51. https://doi.org/10.1016/j.ijhydene.2014.12.103.
[52] Liu D, Wang Y, Shi D, Jia X, Wang X, Borgna A, et al. Methane reforming with carbon dioxide over a Ni/ZiO2-SiO2 catalyst: influence of pretreatment gas atmospheres. Int J Hydrogen Energy 2012;37:10135–44. https://doi.org/10.1016/j.ijhydene.2012.03.158.
[53] Wang LC, He L, Liu YM, Cao Y, He HY, Fan KN, et al. Effect of pretreatment atmosphere on CO oxidation over α-Mn2O3 supported gold catalysts. J Catal 2009;264:145–53. https://doi.org/10.1016/j.jcat.2009.04.006.
[54] de Sousa HS A, da Silva AN, Castro AJR, Campos A, Filho JM, Oliveira AC. Mesoporous catalysts for dry reforming of methane: correlation between structure and deactivation behaviour of Ni-containing catalysts. Int J Hydrogen Energy 2012;37:12281–91. https://doi.org/10.1016/j.ijhydene.2012.05.151.
[55] Makri MM, Vasiliades MA, Petallidou KC, Efstathiou AM. Effect of support composition on the origin and reactivity of carbon formed during dry reforming of methane over 5wt% Ni/Ce1−xMxO2−δ (M=Zr4+, Pr3+) catalysts. Catal Today 2015:1–15. https://doi.org/10.1016/j.cattod.2015.06.010.
[56] Zhang J, Li F. Coke-resistant Ni@SiO2 catalyst for dry reforming of methane. Appl Catal B Environ 2015;176–177:513–21. https://doi.org/10.1016/j.apcatb.2015.04.039.
[57] Rezaei M, Alavi SM, Sahebdelfar S, Bai P, Liu X, Yan ZF. CO2 reforming of CH4 over nanocrystalline zirconia-supported nickel catalysts. Appl Catal B Environ 2008;77:346–54. https://doi.org/10.1016/j.apcatb.2007.08.004.
[58] Juan-Juan J, Román-Martínez MC, Illán-Gómez MJ. Effect of potassium content in the activity of K-promoted Ni/Al2O3 catalysts for the dry reforming of methane. Appl Catal A Gen 2006;301:9–15. https://doi.org/10.1016/j.apcata.2005.11.006.
[59] Alipour Z, Rezaei M, Meshkani F. Effect of alkaline earth promoters (MgO, CaO, and BaO) on the activity and coke formation of Ni catalysts supported on nanocrystalline Al2O3 in dry reforming of methane. J Ind Eng Chem 2014;20:2858–63. https://doi.org/10.1016/j.jiec.2013.11.018.
[60] Odedairo T, Chen J, Zhu Z. Metal-support interface of a novel Ni-CeO2 catalyst for dry reforming of methane. Catal Commun 2013;31:25–31. https://doi.org/10.1016/j.catcom.2012.11.008.